International Journal of Heat and Mass Transfer 52 (2009) 5682–5690

Contents lists available at ScienceDirect

International Journal of Heat and Mass Transfer

journal homepage: www.elsevier.com/locate/ijhmt

Traveling void wave in horizontal two-phase flow

Takeyuki Ami [a,1], Hisashi Umekawa [a,1], Mamoru Ozawa [a,*], Masahiro Shoji [b,2]

[a] Department of Mechanical Engineering, Kansai University, Yamate-cho 3-3-35, Suita, Osaka 564-8680, Japan
[b] Department of Mechanical Engineering, Kanagawa University, Rokkaku-bashi 3-27-1, Kanagawa-ku, Yokahama 221-8686, Japan

ARTICLE INFO

Article history:
Received 24 December 2008
Received in revised form 27 July 2009
Accepted 26 August 2009
Available online 19 September 2009

Keywords:
Two-phase flow
Flow pattern
Void wave
Discrete bubble model
Pattern dynamics

ABSTRACT

In the framework of pattern dynamics approach, the discrete bubble model was developed for simulating inherent fluctuation of void fraction in a horizontal two-phase flow. Then flow patterns were identified based on the statistical properties of void fraction fluctuation, and the flow pattern map agreed with the experimental observation of high-pressure two-phase flow of CO_2 in horizontal tubes. The time-averaged pressure drop and the void fraction obtained in the simulation agreed reasonably with the existing correlations. Thus the horizontal flow version of the discrete bubble model demonstrates its relevance in simulating inherent fluctuation of two-phase flow.

1. Introduction

Two-phase flow is a very complex flow due to the existence of interface between gas and liquid phases. The complexity is mainly brought about by deformation of the interface, coalescence and splitting of bubbles. An instantaneous geometrical configuration of such interface, i.e. a frozen image of interfaces or geometrical structure, is referred to as "flow pattern". Each flow pattern has unique characteristics, and thus is closely related to boiling heat transfer, that is a very important design factor of two-phase flow systems, such as boiler, BWR, SG of PWR and other heat exchangers with phase change. Based on huge amount of investigations in the past five to six decades, a variety of correlations and simulation codes, e.g. RELAP and TRAC based on two-fluid model [1], are now available in planning and/or design stages of two-phase systems.

As is well known, a principal and typical feature of two-phase flow is the inherent fluctuations of pressure and void fraction caused by the existence of interface and its geometrical configuration. When a high heat flux is imposed on such a two-phase system, this inherent fluctuation may cause a critical heat flux condition and other unfavorable events [2]. So far proposed models such as drift-flux model and two-fluid model are formulated based on time-averaged properties [1]. This time-averaging is conducted over a short period so as to be available in simulating transient thermal-flow behavior with the time constant of an order of residence time through a concerned element of two-phase flow system, but over a long period so as to smooth local/instantaneous fluctuation and discontinuity of parameters, so that the velocities of both phases are defined everywhere in time and space. Thus the code has no capability to simulate inherent fluctuation of two-phase flow. In simulating two-phase flow with e.g. two-fluid model, we need many correlations specified to each flow pattern, and flow pattern transition criteria as well. In order to include detailed structure, we would need further detailed correlations and/or closure relationships. An increase in the number of correlations in simulating complex properties results in a decrease in the flexibility of the model, and obstructs rather than enhances an appearance of complexity. In order to gain insight into the complexity in two-phase flow and inherent fluctuation, an alternative approach is indispensable.

Focusing on the behavior of bubbles and induced flow structure including turbulence, numerical simulations have been conducted with so-called interface-tracking simulation [3], including, e.g. front-tracking, VOF, phase-field modeling, level-set, and a variety of applications have been reported. These simulations have, however, difficulty in simulating whole boiling channel system, and the transient behavior such as flow oscillation is far beyond the scope.

Considering the complexity in two-phase flow, an alternative approach with e.g. CA (cellular automata) and coupled-map lattice may be applicable, while realistic images might be harmed due to the use of metaphor model. In order to simulate instantaneous fluctuations of the void fraction and to know the statistical

* Corresponding author. Tel./fax: +81 6 6368 0807.
E-mail addresses: umekawa@ipcku.kansai-u.ac.jp (H. Umekawa), ozawa@ipcku.kansai-u.ac.jp (M. Ozawa), shoji@kanagawa-u.ac.jp (M. Shoji).
[1] Tel./fax: +81 6 6368 0804.
[2] Tel.: +81 45 481 5661x3371; fax: +81 45 481 5122.

0017-9310/$ - see front matter © 2009 Elsevier Ltd. All rights reserved.
doi:10.1016/j.ijheatmasstransfer.2009.08.018

properties unique to each flow pattern, a pattern dynamics model has been developed by the authors based on the void-propagation equation, i.e. mass conservation equation of gas phase and a limited number of local rules representing momentum effects [4–6]. The developed model is referred to as "discrete bubble model" by the authors. These previous works aimed to simulate isothermal two-phase flow in a vertical tube, and the simulation results well demonstrated the void fraction fluctuation as well as the specific statistical properties of each flow pattern, i.e. bubbly, slug, churn and annular flows.

This discrete bubble model has been expanded to become available in a horizontal two-phase flow simulation, and in this paper the discussion is mainly focused on newly developed items for horizontal flow simulation. Then finally the high potential of the proposed model is demonstrated through a comparison with the experimental observation of flow patterns.

2. Discrete bubble model

Fundamental concepts of the newly developed discrete bubble model for horizontal flow is, in principle, the same as the previously proposed vertical flow model. The new development is focused on the pressure and the slip relationships suitable to a horizontal flow condition, and the rests are unchanged.

2.1. Flow model

The flow field is one-dimensional isothermal horizontal two-phase flow as illustrated in Fig. 1. A liquid is supplied from the left end, and a gas is injected through a gas-injection section of length L_M. Two-phase mixture generated in this section flows through the tube towards the right-end and is ejected to an ambient space at the system pressure.

In the discrete bubble model, the flow field is divided into cylindrical cells with the same length as the tube diameter, and this cylindrical cell is used as the frame of reference. Then the spatial resolution of the present model is limited to this unit cell size. A single hypothetical bubble located in the cell center is defined as a volume geometrically similar to the unit cell as shown in Fig. 2. Then the void fraction ε_G in the cell is given by Eq. (1).

$$\varepsilon_G = \left(\frac{D_B}{D_P}\right)^3 \tag{1}$$

where D_B is the diameter of the single hypothetical bubble and D_P is the diameter of tube. Although the present model is one-dimensional, the hypothetical bubble is introduced in defining various local rules including void fraction, bubble induced wake, pressure drop and so on. The geometrical similarity of the hypothetical bubble to the unit cell is not an essential factor, while this hypothesis together with the definition of the unit cell makes the formulation rather simple. Once accepted these hypotheses, each flow pattern is represented as a bubble train as demonstrated in Fig. 3, where the left column represents images of geometrical configuration of the interface and the right column corresponding bubble train aligned along the tube.

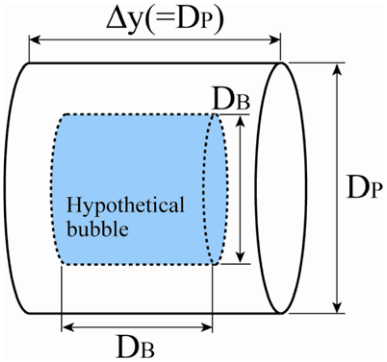

Fig. 2. Single bubble hypothesis.

In view of whole flow field during steady and/or slow transient conditions, gas compressibility plays a minor role in the void-propagation. Thus the spatio-temporal behavior of void fraction in one-dimensional flow field is represented with a void-propagation equation, Eq. (2), for incompressible flow.

$$\frac{\partial \varepsilon_G}{\partial t} + \frac{\partial (\varepsilon_G U_G)}{\partial y} = q \tag{2}$$

where U_G is a velocity of gas phase, t and y represents time and an axial coordinate, respectively, q is a source term of gas phase and is given as a function of a volumetric flux J_G of gas phase, $q = J_G/L_M$, in the gas-injection section, while $q = 0$ outside the injection section. In a boiling channel, this source term is given by the vapor generation rate per unit volume. When a phase change or boiling takes place throughout the tube, the source term is distributed along the tube.

This void-propagation equation is applied over the whole flow field as a global rule. In order to simulate dynamic behavior, such as bubble coalescence, breakup, expansion and/or compression leading to flow pattern transition, it is essential to take into account momentum effects exerted on the hypothetical bubble. Such momentum effects are included as local rules, being the same as in the previous paper [5,6]. In the following sections, details of these local rules are described, while focusing on newly introduced and/or improved items for the horizontal flow simulation. The detailed structure of the model can be also found elsewhere [5,6].

2.2. Relative velocity between gas and liquid phases

Provided the local drift velocity u_{GJ} with respect to the center of volume of the mixture J_T, the velocity of gas phase U_G is given by [1]

$$U_G = J_T + u_{GJ} = J_G + J_L + u_{GJ} \tag{3}$$

where J_L is a volumetric liquid flux. The drift velocity of gas phase is a function of the void fraction ε_G and the slip velocity u_r as follows.

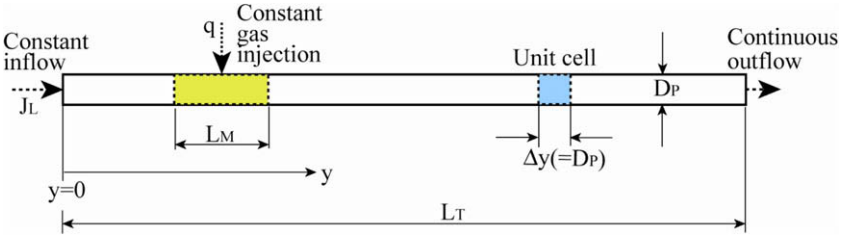

Fig. 1. Flow model.

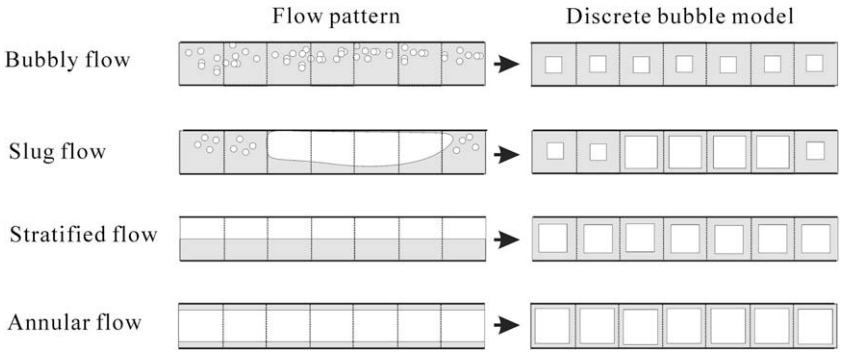

Fig. 3. Flow configurations, left column: actual image, right column: model image.

$$u_{GJ} = (1-\varepsilon_G)u_r = (1-\varepsilon_G)(U_G - U_L) \tag{4}$$

where U_L is a velocity of liquid phase. Although these local relationships are integrated across the tube cross-section to give the distribution parameter and the weighted-mean drift velocity in general purposes, the present model still employs Eqs. (3) and (4) in the present form with respect to universal application to all flow patterns.

The slip velocity used in the vertical flow model was given with a terminal velocity of bubble in a stationary liquid. In the present horizontal flow, this terminal velocity corresponds to the velocity of air cavity during a discharging process of liquid into an ambient air out of a liquid-filled horizontal tube closed at one end. Such a phenomenon is referred to as the "gravity current", and was analyzed by Benjamin [7]. In a small-bore tube with flowing liquid, the velocity of air cavity suffers from an effect of momentum flux as well as the surface tension, and is given by Weber [8] and Sakaguchi et al. [9],

$$u_r = \sqrt{\frac{gD_p(\rho_L-\rho_G)}{\rho_L}}\{0.542 - 1.76Bo^{-0.56}\} \tag{5}$$

where the dimensionless number $Bo \equiv (\rho_L-\rho_G)gD_P^2/\sigma$ denotes the Bond number, g is the acceleration of gravity, ρ_L and ρ_G are densities of liquid and gas phases, respectively, and σ is a surface tension. The first term in the parenthesis of right-hand side in Eq. (5) corresponds to Benjamin's solution, i.e. the cavity velocity without the effect of surface tension. This equation implies that the cavity velocity, i.e. the slip velocity in the present case, becomes zero beyond $Bo = 8.19$. This Eq. (5) is extensively used for simplicity of the numerical simulation in the whole range of the present investigation, although the gravity current phenomena may be limited only in the plug and slug flows.

2.3. Wake effect of preceding bubble

When two bubbles move successively, a succeeding bubble is influenced by the wake of a preceding bubble. The succeeding bubble catches up with the preceding bubble, and these two bubbles coalesce into one large bubble. Such a feature is often observed in a vertical flow, and may be consistent in a horizontal flow as well. Thus the same relationship as the vertical flow model is used in estimating the wake velocity.

$$u_{w,\max,i} = c_1 u_{r,i+1}\left(\frac{C_D D_{B,i+1}^2}{\Delta y^2}\right)^{1/3} \quad (\varepsilon_{G,i+1} \geqslant \varepsilon_{G,i})$$
$$u_{w,\max,i} = 0 \quad (\varepsilon_{G,i+1} < \varepsilon_{G,i}) \tag{6}$$

where C_D (=0.44) is a drag coefficient, c_1 is a constant, $c_1 = 0.715$, Δy the length of unit cell, and suffix i and $i+1$ the cell numbers as illustrated in Fig. 4. Eq. (6) is based on the relationship for circular wake by Schlichting [10]. This equation gives a maximum wake velocity in the ith cell caused by the bubble in the $i+1$th cell. Just as the same manner as the vertical flow model, the wake effect exerted on the bubble in the ith cell is given by an integration over the length $c_3 \times \Delta y$ ahead of the concerned bubble,

$$u_{w,i} = u_{w,\max,i} + \sum_{j=1}^{c_3} u_{w,\max,i+j}\exp\{-c_2(j+1)\} \tag{7}$$

where c_2 and c_3 are constants, $c_2 = 0.14$ and $c_3 = 20$, respectively (also Refs. [5,6]). The assumed decay process is exemplified in Fig. 5. When tube diameter $D_P = 6.0$ mm is the case, the integration is conducted over 120 mm, i.e. 20 cells, while the wake velocity damps to 25% in the first 10 cells, i.e. 60 mm.

Thus obtained wake velocity is substituted into Eq. (8) to give the slip velocity.

$$u_{r,i+1} = u_{w,i}\left\{c_1\left(\frac{C_D D_{B,i+1}^2}{\Delta y^2}\right)^{1/3}\right\}^{-1} \quad (u_{w,i} > 0) \tag{8}$$

The constants c_1–c_3 and the drag coefficient C_D retain the same respective value, regardless the fluid properties, flow conditions and flow orientations. This is mainly because the present model aims at realizing principal feature of flow pattern formation, but not obtaining exact solutions.

2.4. Compressibility of gas phase

In spite of the discussion in Section 2.1, the gas compressibility plays, in reality, an important role in a local and instantaneous bubble behavior. In other words, bubbles move with expanding or compressing, even though weakly, in accordance with the local pressure, and these fluctuations of bubble, i.e. void fraction fluctuation, show substantial importance in the formation of intermittent flow pattern [5,6,11]. An inclusion of gas compressibility

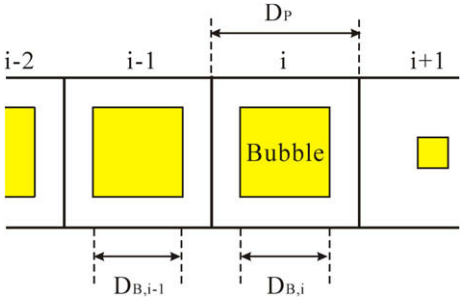

Fig. 4. Cell system.

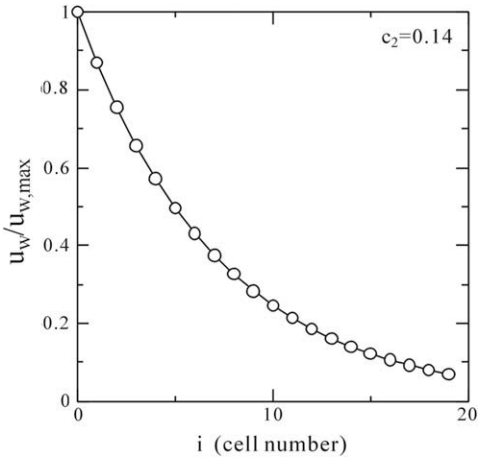

Fig. 5. Decay of wake velocity.

mechanism in local rules, as a matter of course, gives rise to an inconsistency with Eq. (2) of incompressible flows. This inconsistency is covered with the calculation sequence as described in Section 3.

Provided isothermal state change of the hypothetical bubble in the *i*th cell, we obtain

$$V_{B,i}^{n+1} = V_{B,i}^{n}(p_i^n/p_i^{n+1}) \tag{9}$$

where V_B is a volume of bubble, p is a static pressure and superscript n and $n+1$ denote nth and $n+1$th time steps, respectively. The local pressure is given as an integral of cell-to-cell pressure difference from the exit of the tube to the designated location.

Ozawa et al. [12] and Sakaguchi et al. [13] analyzed a slug flow in a horizontal tube on the basis of the regime-based modeling shown in Fig. 6. The liquid slug travels with the scooping of liquid and momentum ahead of the liquid slug, and shedding liquid below the large bubble at the tail of liquid slug. This mechanism is referred to as the scooping-shedding mechanism [14].

One-dimensional mass and momentum conservations with moving boundary are given with a help of Leibniz rule [12,13,15],

$$\frac{d}{dt}\int_V \rho dv + \int_A \rho\{(\boldsymbol{U}-\boldsymbol{U}_a)\cdot\boldsymbol{n}\}da = 0 \tag{10}$$

$$\frac{d}{dt}\int_V \rho\boldsymbol{U}dv + \int_A \rho\boldsymbol{U}\{(\boldsymbol{U}-\boldsymbol{U}_a)\cdot\boldsymbol{n}da = -\int_A p\boldsymbol{n}da + \int_V \nabla\cdot\tau dv \tag{11}$$

where ρ is a density, $\boldsymbol{U}$ a velocity vector, $\boldsymbol{U}_a$ a velocity vector of moving boundary, $\boldsymbol{n}$ a unit vector normal to the interface, $\boldsymbol{\tau}$ a viscous stress tensor, V a volume of reference body and A the interfacial area. In a vertical flow model, the gravity term is needed in the right-hand side of Eq. (11). In the framework of one-dimensional flow, these equations are applied to the liquid-scooping region, main body of the liquid slug and the liquid-shedding region, respectively, where the first and the third regions are considered as a kinematic shock wave [16], and quasi-steady relationships are provided.

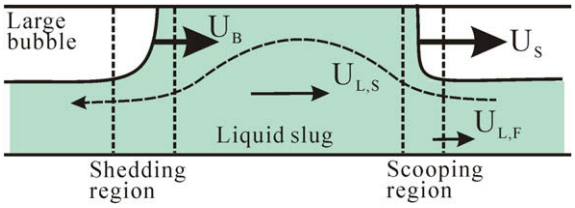

Fig. 6. Regime-based slug flow modeling.

Then the liquid slug behavior is given, under the assumption of uniform liquid holdup in the slug, by

$$\frac{d(\rho_L\varepsilon_L L_S)}{dt} + \varepsilon_L\rho_L(U_B - U_S) = 0 \tag{12}$$

$$p_F - p_R = \frac{d}{dt}(\rho_L\varepsilon_{L,S}U_{L,S}L_S) + \Delta p_f + \varepsilon_{L,F}\rho_L U_{L,F}(U_{L,F} - U_S) - \varepsilon_L\rho_L U_{L,S}(U_{L,S} - U_B) \tag{13}$$

where Δp_f a frictional pressure drop across the reference volume, ε_L the liquid hold-up ($=1-\varepsilon_G$), L_S the liquid slug length, U_L the liquid velocity, U_S and U_B the liquid slug velocity and the large bubble velocity. Subscripts *F*, *R* and *S* denote the scooping region, the shedding region and the liquid slug, respectively. Although these equations have been derived for a macro-scale slug flow, the similar relationships are provided in formulating cell-to-cell pressure difference in the discrete bubble system. Thus the original equation (13) is modified so as to be applicable to the discrete bubble model under the quasi-steady assumption.

$$p_i - p_{i+1} = \Delta p_{f,i} - \rho_L g(\varepsilon_{L,i}H_{eq,i} - \varepsilon_{L,i+1}H_{eq,i+1})/2 + \varepsilon_{L,i+1}\rho_L U_{L,i+1}(U_{L,i+1} - U_{G,i+1}) - \varepsilon_{L,i}\rho_L U_{L,i}(U_{L,i} - U_{G,i}) \tag{14}$$

where the liquid slug velocity U_S is assumed equal to the large bubble velocity U_B, and these velocities are further assumed equal to the velocity of gas phase U_G. Due to this simplification, Eq. (12) becomes not in need in discussing the pressure difference. The first term of right-hand side in Eq. (14) corresponds to the frictional pressure drop between successive cells. The second term containing the equivalent liquid height H_{eq} represents the static pressure difference caused by the difference in liquid heights across two successive cross-sections, and the third and fourth terms represent the scooped and shed momentums at the nose and the tail of the liquid slug, respectively.

Compared with the previous paper for a vertical flow [5,6], the second to fourth terms are newly introduced in estimating the pressure difference instead of the gravitational pressure drop along the tube axis. The third and fourth terms are not limited to a horizontal flow, but are rather small compared with the gravitational pressure drop in a vertical flow.

The frictional pressure drop is estimated as a sum of the part of liquid phase Δp_L and the part of the large bubble Δp_B.

$$\Delta p_f = \Delta p_L + \Delta p_B = \lambda_L\frac{D_P - D_B}{2D_P}\rho_L U_L|U_L| + \lambda_B\frac{D_B}{2D_P}\rho_L U_L|U_L| \tag{15}$$

where a wall friction factor λ_L is given by Hagen-Poiseuille equation in a laminar flow and Blasius equation in a turbulent flow, and the friction factor of the second term is set constant $\lambda_B = 0.02$ as given by Wallis' annular model [17]. It is noted that variables in Eq. (15) and next Eq. (16) are expressed without suffix *i*, but are defined in each cell.

The equivalent liquid height in the right-hand side of Eq. (14) is calculated simply by the substitution of a stratified flow model shown in Fig. 7 [9,13], neglecting the geometrical configuration of bubble provided in the present model.

$$\varepsilon_L H_{eq}/2 = \frac{1}{A_C}\int_0^h yL_C dy \tag{16}$$

where

$$L_C = D_P\cos\phi, \quad h = D_P(1+\sin\phi)/2, \quad \varepsilon_L = (\pi + 2\phi + \sin 2\phi)/2\pi$$

and A_C is the tube cross-section, y is the distance from a gas–liquid interface, L_C is the chord length, h is the height of the interface, and ϕ is the angle of the interface.

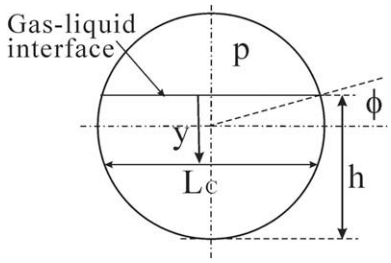

Fig. 7. Definition of equivalent liquid height.

2.5. Phase re-distribution for geometrical consistency

When a bubble expands due to the pressure change, the volume of the bubble happens to exceed beyond the volume of the unit cell. In order to avoid such inconsistency, a limiting value of the void fraction $\varepsilon_{G,cr}$ is predetermined, and the excess amount $\Delta\varepsilon_{G,i} = \varepsilon_{G,i} - \varepsilon_{G,cr}$ beyond this limiting value is compensated through the phase re-distribution process to the downstream cell. Instead, a part of surplus liquid hold-up $\Delta\varepsilon_{L,i}$ pushed out of the downstream cell is uniformly re-distributed to upstream cells as illustrated in Fig. 8. The re-distributed liquid hold-up $\delta\varepsilon_{L,i}$ into each cell is assumed to be a function of limiting value of void fraction as follows:

$$\delta\varepsilon_{L,i} = \Delta\varepsilon_{L,i}/i = \{-\Delta\varepsilon_{G,i}\exp(-c_4\varepsilon_{G,cr})\}/i \quad (17)$$

where c_4 is set constant, $c_4 = 5$, and the limiting void fraction $\varepsilon_{G,cr}$ is also constant, $\varepsilon_{G,cr} = 0.95$ throughout the simulation. Moreover these values are the same as those of the vertical flow model. Then the exponential term is rather small, 0.087. Thus, only a minor part of liquid corresponding to the excess void fraction is re-distributed upstream, and most of the surplus liquid is pushed downstream. Such a functional relationship is artificial, while it seems not so peculiar when observing the behavior of a large bubble and the surrounding liquid during transient states. This phase re-distribution process is rather important in the transition process of intermittent to annular flow.

3. Numerical simulation

The numerical simulation was conducted with a finite-difference method. A staggered-mesh system is applied, i.e. the void fraction and the pressure are defined at the center of the unit cell, and the velocity on the boundary of the cell. A time derivative and convection term in the finite-difference equation were expressed with a forward difference and an upwind difference, respectively. Constant inflows of liquid and gas are set at the inlet, and continuous outflow at the right-end exit as shown in Fig. 1 in the present simulation. These boundary conditions are not definite ones, but may be given, e.g. as a function of time.

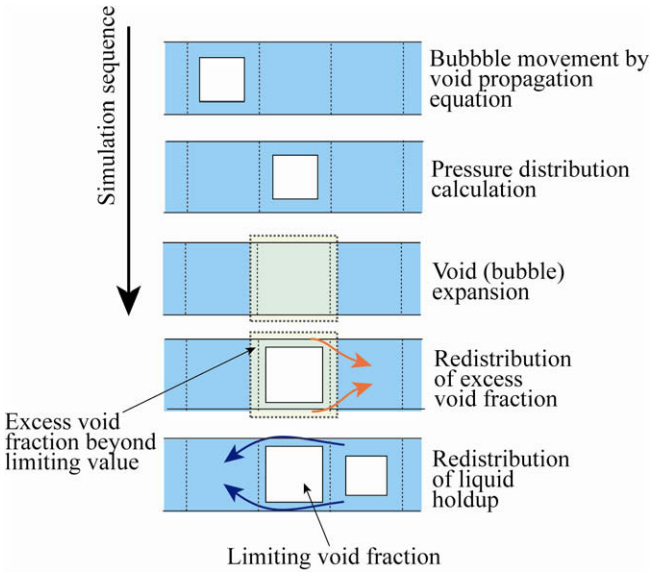

Fig. 8. Sequence of simulation.

The simulation sequence is simply illustrated in Fig. 8: first, the hypothetical bubble movement, i.e. provisional void fraction distribution, is calculated with the void-propagation equation, Eq. (2), and then the pressure distribution is calculated, so that the volume expansion or compression is determined. The excess void fraction and corresponding surplus liquid holdup are re-distributed. Thus obtained void fraction is recorded as the definite value at a designated time step, and the simulation proceeds to the next time step.

Aiming at the verification of the present horizontal flow model, the simulation condition and the system configurations are selected as shown in Table 1 so that the flow pattern maps are compared with the experiment by the authors [18,19].

3.1. Void fraction fluctuation and flow pattern map

Prior to describing simulation results, a brief explanation on the experiment is given here. Experimental investigations were conducted with a forced-flow boiling system of CO_2 shown in Fig. 9. Experimental setup consists of CO_2 pump, a pre-cooler, a test section of 2.0 mm in inner diameter with Joule heating, a sight glass for flow pattern observation, an exhaust gas heater and a laminar flowmeter. Operating pressure was in the range 4.0–6.7 MPa, mass flux was ranging from 200 to 700 kg/m^{2}s, and vapor quality 0.05–0.9. Detailed description may be found elsewhere [18,19].

Typical flow patterns observed at 6.5 MPa are shown in Fig. 10. Each flow pattern has the following features, being used in the flow pattern identification in the experiments:

Bubbly flow: dispersed small bubbles,
Plug flow: slow-moving elongated bubbles at relatively low void fraction,
Slug flow: intermittent large-scale liquid slugs and large bubbles,
Annular flow: gas core surrounded with thin liquid film, often with entrainments,
Slug-annular flow: gas flow penetrating through the liquid slug, and
Wavy-annular flow: annular flows with rather thick and wavy liquid layer at the bottom.

Further increase in the gas velocity beyond the wavy-annular flow brings about an appearance of liquid entrainment above the wavy interface. Such a flow pattern is referred to as the wavy-mist flow which is, however, not shown in Fig. 10.

Table 1
Simulation conditions.

Working fluid	CO_2
System pressure, p	6.5 MPa
Mass flux, G	50–800 kg/m^{2}s
Quality, x	0.01–0.9
Total length of tube, L_T	400 mm
Mixing chamber length, L_M	20 mm
Pressure drop measurement, L_P	200 mm
Tube diameter, D_P	2.0 mm
Unit cell length, Δy	2.0 mm
Number of cells, GN	200
Time step, Δt	0.01 ms

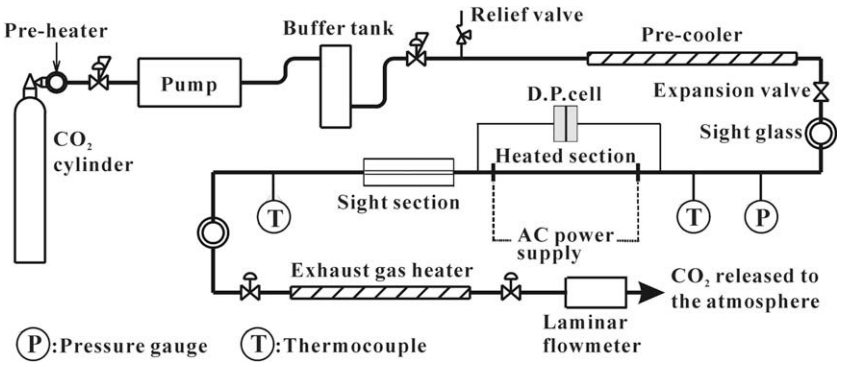

Fig. 9. Experimental setup of forced-flow boiling of CO_2.

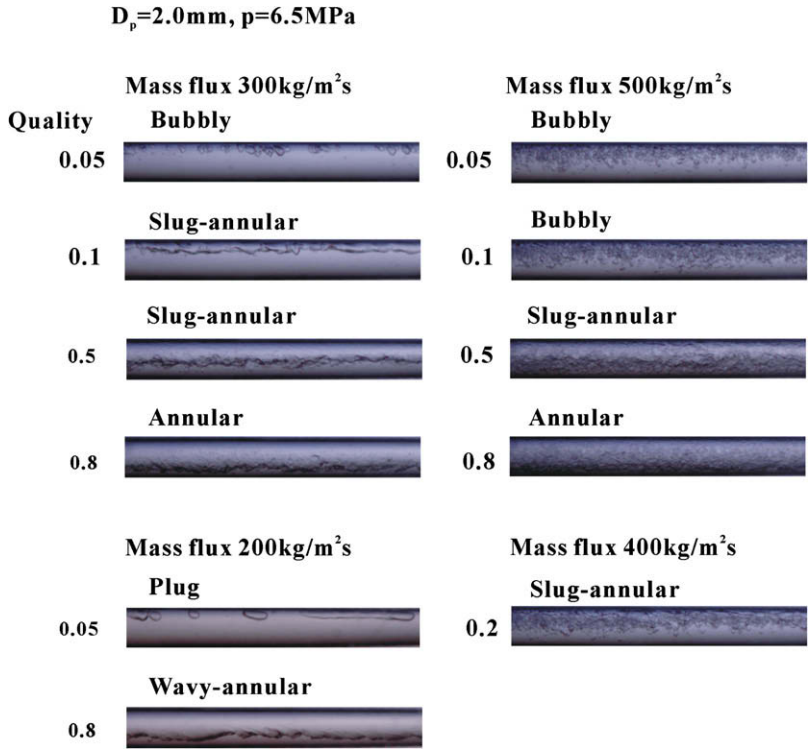

Fig. 10. Observed flow patterns in the experiment with CO_2 at 6.5 MPa in 2.0-mm tube.

In the following, simulation results are described with emphasis on the flow pattern. Typical snapshots of the void fraction distribution are shown as a function of the axial coordinate in Fig. 11(a) together with the representative probability density functions (PDF) in Fig. 11(b) detected at the middle position, $y = 0.222$ m, along the tube. Two vertical lines at the left end in the snapshot represent the gas injection region. Flow conditions, mass flux G and quality x, are indicated in each PDF. Simulation results show, in part, similar to those in the vertical flow. The first one shown in Fig. 11(a)-1 ($G = 50$ kg/m^{2}s, $x = 0.01$) belongs to this group: there is ripple-like void fraction fluctuation, i.e. void wave, traveling along the tube. Corresponding PDF has a single peak at low void fraction as shown in Fig. 11(b)-1. This void fluctuation pattern corresponds to bubbly flow, similarly to the vertical flow [5,6,20].

Increased vapor quality as shown in the case of Fig. 11(a)-2 ($G = 50$ kg/m^{2}s, $x = 0.1$), relatively large void waves, corresponding to large bubbles, are formed intermittently along the tube. Then the PDF has two peaks at both low and high void fractions. This flow pattern is considered as slug flow.

At rather high quality as shown in Fig. 11(a)-3 ($G = 300$ kg/m^{2}s, $x = 0.9$), the void fraction becomes rather uniform, keeping almost equal value to the pre-determined limiting void fraction. The PDF has a single peak at high void fraction as shown in Fig. 11(b)-3. This flow pattern corresponds to annular flow.

The next group of the flow patterns are those appeared uniquely in this horizontal flow model. In Fig. 11(a)-4 ($G = 300$ kg/m^{2}s, $x = 0.2$), the void fraction has a sinuous distribution along the tube, but is limited within a moderate range. Corresponding PDF has two peaks like a slug flow as in Fig. 11(b)-4, while the amplitude is relatively small compared with the slug flow. This type of flow seems a transition from slug to annular flow, and corresponds to slug-annular flow.

In the last column, Fig. 11(a)-5 ($G = 50$ kg/m^{2}s, $x = 0.8$), the void fraction is rather high at the wave crest, but with rather low value in-between successive two wave crests. With reference to the holdup, the flow behavior seems annular flow but with large amplitude waves. The existence of this large wave results in the PDF with two peaks shown in Fig. 11(b)-5. This flow pattern corresponds to wavy-annular flow.

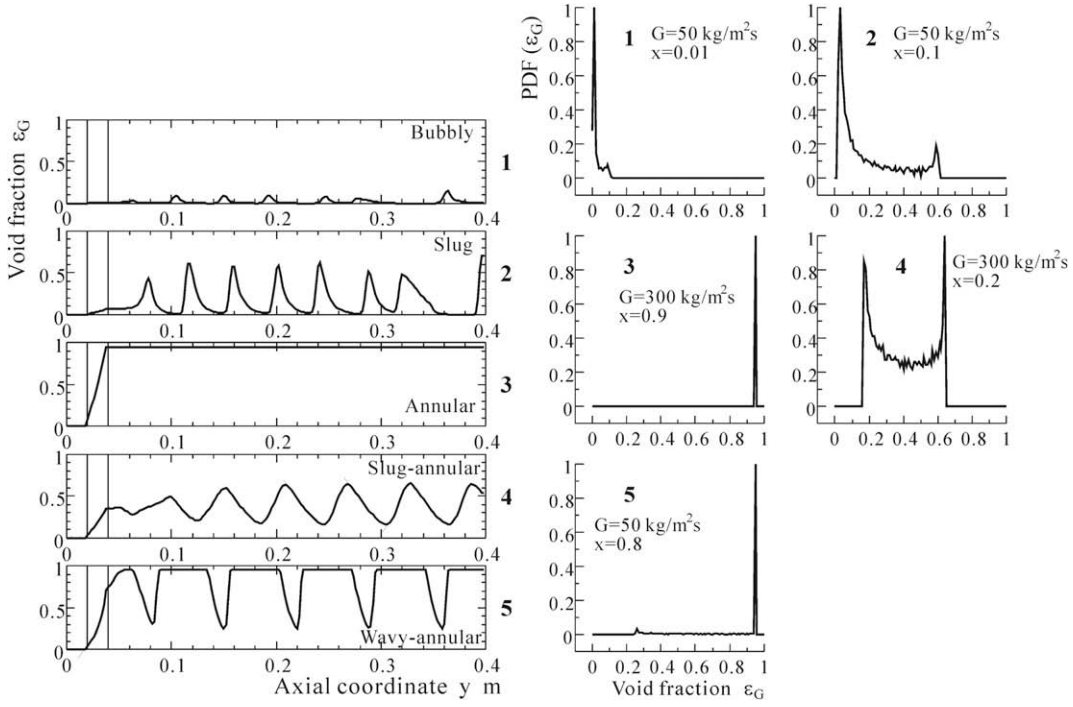

Fig. 11. Void fraction fluctuation and PDF: (a) snap shot of void fraction distribution and (b) corresponding PDF, (p = 6.5 MPa).

Most of the typical features observed in the numerical simulation well correspond to the flow patterns in the experiment. In identifying the flow patterns from the numerical simulation data, plug flow is hard to classify, and may be included either in bubbly flow or in slug flow, depending on the amplitude of void fraction fluctuation. In addition, the wavy-annular flow in the simulation may include wavy and wavy-mist flows. This is mainly because the present simulation is based on the one-dimensional flow model and then insensible to the phase distribution across the tube cross-section. From this context, a mist flow is quite different in the arrangement of phases from the pre-determined hypothetical bubble system shown in Fig. 2, and thus out of scope of the present model, although mist flow was observed in the experiment at very high quality at lower pressure, 5.0 MPa [18,19].

The flow pattern identification of the simulation results are conducted, in principle, based on the above-mentioned typical features, being similar to Jones and Zuber [20], and the simulation results for vertical flow [5,6], while the slug-annular as well as the wavy-annular patterns, in particular, needs additional threshold conditions. Then the flow pattern-transition criteria were determined with a maximum ($\varepsilon_{G,\max}$) and a minimum ($\varepsilon_{G,\min}$) void fractions, together with the above-mentioned typical features:

$$\begin{aligned}
&\text{Bubbly flow}: && \varepsilon_{G,\min} < 0.1, \varepsilon_{G,\max} < 0.6 \\
&\text{Slug flow}: && \varepsilon_{G,\min} < 0.1, \varepsilon_{G,\max} \geqslant 0.6 \\
&\text{Annular flow}: && \varepsilon_{G,\min} \geqslant 0.8 \\
&\text{Slug-annular flow}: && 0.1 < \varepsilon_{G,\min} < 0.8, \varepsilon_{G,\max} < 0.9 \\
&\text{Wavy-annular flow}: && 0.1 < \varepsilon_{G,\min} < 0.6, \varepsilon_{G,\max} \geqslant 0.9
\end{aligned} \tag{18}$$

Thus identified flow pattern map (lower column) are plotted as a function of mass flux and quality in Fig. 12 together with the experimental result (upper column) [18,19]. In these flow pattern maps, so far proposed flow pattern transition criteria are also drawn for reference: solid lines by Cheng et al. [21] developed for CO_2 with ordinary tube size (tube diameters from 0.6 to 10 mm), and the dashed lines by Revellin and Thome [22] for micro-channels, where symbol "IB" denotes isolated bubble regime, "CB" coalescing bubble regime, and "A" annular flow regime. In comparison with the experimental observation, the predicted regions for bubbly flow, annular flow, and the transition patterns, i.e. slug-annular and wavy-annular flows, coincide approximately with the experiment. In addition, the slug-annular flow in the simulation penetrates into the predicted annular flow region, which is quite similar to the experimental observation. The slug flow occupying low mass flux region of the

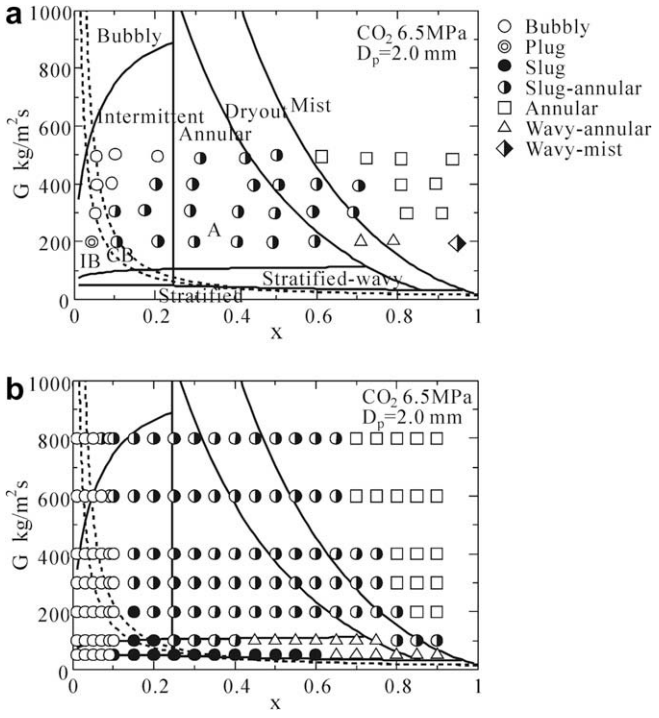

Fig. 12. Flow pattern map: (a) experiment; (b) simulation, solid lines: Cheng et al. [21], dashed lines: Revellin and Thome [22], IB: isolated bubble regime, CB: coalescing bubble regime and A: annular flow regime.

simulation has not been observed in the experiment due to the limitation of the pump performance, while experimental data at 5.0 MPa suggest an availability of the present model [19] for slug flow as well. Detailed discussion on the comparison with the existing criteria may be found elsewhere [19].

To demonstrate further verification of the present model, comparison with the flow pattern map shown in the upper column of Fig. 13 by Schael and Kind [23] is conducted. Schael and Kind observed flow patterns of CO_2 at 2.64 MPa, being at lower pressure than the present case, but with micro-fin tube of 8.62 mm in diameter. They identified bubbly, slug, slug-annular similarly to the present paper, annular, wavy-annular, wavy and stratified-wavy flows, while in Fig. 13 the wavy and the stratified-wavy flows at low mass flux are included in the same category of stratified-wavy flow. Curves drawn for reference in the figure are of Cheng et al. [21]. The simulation result indicates that the slug, slug-annular and annular flows are as a whole in good agreement with the experimental results. This fact suggests that the effect of micro-fin is not significant for the appearance of these dominant flow patterns. It is of course that there exists still a minor difference between the experiment and the simulation, e.g. the plotted stratified-wavy region approximately corresponds to the wavy-annular region in the simulation. On the other hand, the wavy-annular flow region of the experiment seems to be included in the annular flow region of the simulation. At low quality, the wavy-annular region penetrates into the slug-annular region in the simulation, although not in the experiment. This inappropriate appearance of wavy-annular flow may be due to the fact that the present flow pattern identification is based only on the void fraction fluctuation, but not on the geometrical configuration as in the experiment.

As described above, the present model is available to realize the PDF of void fraction fluctuation, i.e. a fluctuation pattern of void fraction being specified to each flow pattern. However, if the model has a capability of not only pattern formation but also quantitative data prediction including pressure drop, void fraction and so on, the present model becomes of great significance in two-phase flow dynamics.

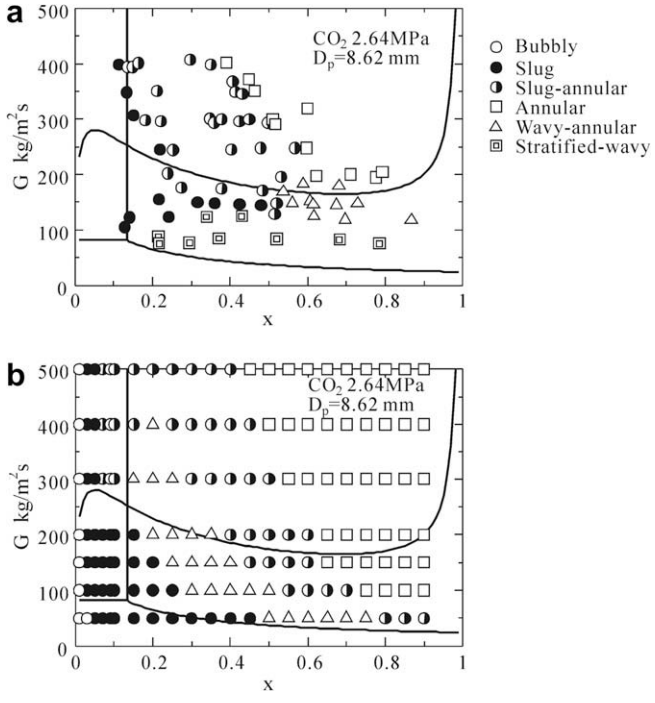

Fig. 13. Flow pattern map: (a) experiment by Schael and Kind [23], courtesy of Prof. M. Kind; (b) simulation, solid lines: Cheng et al. [21].

3.2. Time-averaged characteristics

In this section are discussed the time-averaged properties of pressure drop and void fraction. The time-averaged values are obtained in the fully-developed region. Fig. 14 shows time-averaged pressure drop plotted in the frame-work of Lockhart–Martinelli correlation [24],

$$\phi_L^2 = (\Delta p_f/L_P)/(\Delta p_f/L_P)_L \tag{19}$$

$$\mathrm{X}^2 = (\Delta p_f/L_P)_L/(\Delta p_f/L_P)_G \tag{20}$$

where the pressure drop Δp_f is the time-averaged value, ϕ_L is a two-phase friction multiplier, and X is the Martinelli parameter. The length L_P means a distance for pressure drop calculation. Parentheses $()_L$ and $()_G$ denote single phase flows of liquid and gas, respectively. Lines in this figure are drawn with the following Chisholm's correlation [25].

$$\phi_L^2 = 1 + \frac{C}{\mathrm{X}} + \frac{1}{\mathrm{X}^2} \tag{21}$$

where $C = 21$ if gas and liquid phases are in turbulent flow, denoted by "tt" and, $C = 2$ if both phases are in laminar flow, "vv". Mishima and Hibiki [26] modified Chisholm's parameter so as to be applicable to small-bore tubes given by

$$C = 21 \times [1 - \exp(-0.319 D_P)] \tag{22}$$

where $C = 9.9$ for $D_P = 2$ mm. The pressure drop based on homogeneous flow model is also drawn in this figure. Simulation results are on the whole in good agreement with Chisholm's correlation with $C = 2$. The pressure drop prediction with homogeneous flow model works rather well at such a high-pressure, which is in good agreement with the experimental evidence [18,27].

Fig. 15 shows the time-averaged void fraction as a function of vapor-phase velocity J_G/ε_G and the total volumetric flux J_T. Well-known drift-flux model was first proposed by Zuber and Findlay [28], and was modified by Rouhani and Axelsson [29], and further modification was conducted by Steiner [30] considering an application to horizontal flow as follows:

$$\varepsilon_G = \frac{x}{\rho_G}\left[C_0\left(\frac{x}{\rho_G} + \frac{1-x}{\rho_L}\right) + \frac{u_{GJ}}{G}\right]^{-1} \tag{23}$$

where

$$C_0 = 1 + 0.12(1-x)$$

$$u_{GJ} = 1.18(1-x)\left\{\frac{g\sigma(\rho_L - \rho_G)}{\rho_L^2}\right\}^{0.25} \tag{24}$$

where C_0 is a distribution parameter and u_{GJ} is the drift velocity. Mishima and Hibiki [26] proposed the distribution parameter and the drift velocity as well in application to small-bore tubes.

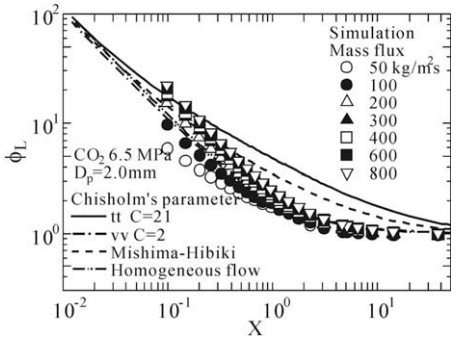

Fig. 14. Correlation of time-averaged pressure drop.

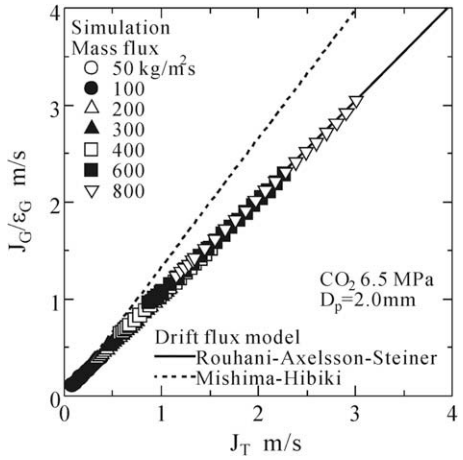

Fig. 15. Correlation of time-averaged void fraction.

$$C_0 = 1.2 + 0.51\exp(-0.691 D_P)$$
$$u_{GJ} = 0 \tag{25}$$

These correlations are drawn with solid and dashed lines, respectively. The time-averaged void fraction well agrees with Rouhani–Axelsson–Steiner correlation. On the other hand, Mishima and Hibiki's correlation deviates significantly from the present data. This is mainly because Mishima and Hibiki's correlation is applicable to so-called mini-channel. On the other hand the present data of high-pressure CO_2 does show macro-channel character but not of mini-channel [17,27].

The above-mentioned comparisons with the existing correlations suggest that the present discrete bubble model for horizontal flows is very effective in predicting not only steady but also unsteady phenomena, including inherent fluctuations, in two-phase flows.

4. Conclusion

The discrete bubble model, previously proposed for a vertical upward flow, was further developed so as to be applicable to the horizontal two-phase flow, and the void fraction fluctuation, i.e. void wave, was successfully simulated. The dominant flow patterns in horizontal flows, i.e. bubbly, slug, slug-annular, annular and wavy-annular flows, were identified with the PDF of the void fraction fluctuation, and the resulting flow pattern maps were in good agreement with the experimental results of CO_2 at high-pressure. Moreover, time-averaged characteristics of frictional pressure drop and void fraction agreed with existing correlations. Based on these evidences, it is concluded that the discrete bubble model gives reasonable void fraction fluctuations in horizontal two-phase flows. Thus, the proposed model gives effective means for simulating transient thermal-flow phenomena, including inherent two-phase flow dynamics.

Acknowledgements

This work was supported by JSPS. KAKENHI (19360104). Authors wish to express sincere thanks to Messrs. T. Yamamoto, Y. Ueda and Y. Tanaka who supported experimental part of this investigation.

References

[1] M. Ishii, T. Hibiki, Thermofluid Dynamics of Two-phase Flow, Springer, New York, 2006.
[2] M. Ozawa, Critical heat flux induced by flow instability in boiling channels, in: Proceedings of the ECI International Conference on Boiling Heat Transfer, Spoleto, 2006, Paper No. KL-2.
[3] N. Takada, M. Misawa, A. Tomiyama, A phase-field method for interface-tracking simulation of two-phase flows, Math. Comput. Simul. 72 (2006) 220–226.
[4] K. Ito, M. Ozawa, M. Shoji, Pattern-dynamics approach to two-phase flow regime transition, in: Proceedings of the Japan-US seminar on Two-Phase Flow Dynamics, vol. 1, Nagahama, 2004, pp. 103–112.
[5] M. Ozawa, T. Ami, H. Umekawa, M. Shoji, Pattern dynamics simulation of void propagation, Multiphase Sci. Technol. 19 (4) (2007) 343–361.
[6] T. Ami, H. Umekawa, M. Ozawa, M. Shoji, Investigation on two-phase flow dynamics with discrete bubble model, Therm. Sci. Eng. 15 (4) (2007) 197–209.
[7] T.B. Benjamin, Gravity currents and related phenomena, J. Fluid Mech. 31 (2) (1968) 209–248.
[8] M.E. Weber, Drift in intermittent two-phase flow in horizontal pipe, Can. J. Chem. Eng. 59 (3) (1981) 398–399.
[9] T. Sakaguchi, M. Ozawa, H. Hamaguchi, T. Fukunaga, Behavior of a large bubble in a horizontal channel (2nd report, Large bubble penetrating into running liquid), Trans. JSME Ser. B 56(527) (1990) 1891–1898.
[10] H. Schlichting, Boundary Layer Theory, Sixth ed., McGraw-Hill, New York, 1968. pp. 685–695.
[11] K. Ito, M. Inoue, M. Ozawa, M. Shoji, A simplified model of gas–liquid two-phase flow pattern transition, Heat Transfer-Asian Res. 33 (7) (2004) 445–461.
[12] M. Ozawa, T. Sakaguchi, H. Hamaguchi, Gas–liquid two-phase transient slug flow modeling, Memoirs of the Faculty of Engineering, Kobe University, vol. 32, 1985, pp. 1–23.
[13] T. Sakaguchi, M. Ozawa, H. Hamaguchi, F. Nishiwaki, E. Fujii, Analysis of the impact force by a transient liquid slug flowing out of a horizontal pipe, Nucl. Eng. Design 99 (1987) 63–71.
[14] A.E. Dukler, M.G. Hubbard, A model for gas–liquid slug flow in horizontal and near horizontal tubes, Ind. Eng. Chem. Fundam. 14 (1975) 337–347.
[15] J.M. Delhay, Instantaneous space-averaged equations, in: J.M. Delhaye, M. Giot, M.L. Riethmuller (Eds.), Thermohydraulics of Two-Phase Systems for Industrial Design and Nuclear Engineering, Hemisphere Pub., New York, 1981, pp. 159–170.
[16] G.B. Whitham, Linear and Nonlinear Waves, John Wiley & Sons, New York, 1974. pp. 26–36.
[17] G.B. Wallis, One-Dimensional Two-Phase Flow, McGraw-Hill, New York, 1969. pp. 323–324.
[18] T. Yamamoto, Y. Ueda, I. Ishihara, M. Ozawa, H. Umekawa, R. Matsumoto, Flow boiling heat transfer of carbon dioxide at high pressure in horizontal mini-channels, in: Proceedings of the Sixth International Conference on Multiphase Flow, Leipzig, 2007, Paper No. S7_Wed_D_44.
[19] M. Ozawa, T. Ami, I. Ishihara, H. Umekawa, R. Matsumoto, Y. Tanaka, T. Yamamoto, Y. Ueda, Flow pattern and boiling heat transfer of CO_2 in horizontal small-bore tubes, Int. J. Multiphase Flow 35 (2009) 699–709.
[20] O.C. Jones Jr., N. Zuber, The interrelation between void fraction fluctuations and flow patterns in two-phase flow, Int. J. Multiphase Flow 2 (1975) 273–306.
[21] L. Cheng, G. Ribatski, J.M. Quibén, J.R. Thome, New prediction methods for CO_2 evaporation inside tubes: part I – A two-phase flow pattern map and a flow pattern based phenomenological model for two-phase flow frictional pressure drop, Int. J. Heat Mass Transfer 51 (2008) 111–124.
[22] R. Revellin, J.R. Thome, A new type of diabatic flow pattern map for boiling heat transfer in microchannels, J. Micromech. Microeng. 17 (2007) 788–796.
[23] A.-.E. Schael, M. Kind, Flow pattern and heat transfer characteristics during flow boiling of CO_2 in a horizontal micro fin tube and comparison with smooth tube data, Int. J. Refrigeration 28 (2005) 1186–1195.
[24] R.W. Lockhart, R.C. Martinelli, Proposed correlation of data for isothermal two-phase, two-component flow in pipes, Chem. Eng. Prog. 45 (1) (1949) 39–48.
[25] D. Chisholm, A theoretical basis for the Lockhart–Martinelli correlation for two-phase flow, Int. J. Heat Mass Transfer 10 (1967) 1767–1778.
[26] K. Mishima, T. Hibiki, Some characteristics of air-water two-phase flow in small diameter vertical tubes, Int. J. Multiphase Flow 22 (4) (1996) 703–712.
[27] M. Ozawa, Flow boiling of carbon dioxide in horizontal mini-channel and pattern dynamics approach to study flow pattern, in: Proceedings of the Seventh International Conference Nanochannels, Microchannels and Minichannels (ICNMM2009), Pohang, 2009, Paper No. 82145.
[28] N. Zuber, J.A. Findlay, Average volumetric concentration in two-phase flow system, Trans. ASME, J. Heat Transfer 87 (1965) 453–468.
[29] S.Z. Rouhani, E. Axelsson, Calculation of void volume fraction in the subcooled and quality boiling regions, Int. J. Heat Mass Transfer 13 (1970) 383–393.
[30] D. Steiner, VDI-Wärmeatlas 7/E, chapter Hbb 6, VDI-Verlag GmbH, Düsseldorf, 1994.